Batteries & Supercaps

Research Article
doi.org/10.1002/batt.202500104

Chemistry Europe
European Chemical Societies Publishing

www.batteries-supercaps.org

# Decoupling Silicon and Graphite Contribution in High-Silicon Content Composite Electrodes

Dimitrios Chatzogiannakis, Ion Ghilescu, Georgia Giannadaki, Marta Cabello, Montse Casas-Cabanas,* and M. Rosa Palacin*

Silicon–graphite (Si/Gr) composite electrodes are widely used in commercial Li-ion batteries to enhance capacity while balancing mechanical stability. This study investigates the electrochemical behavior of high-silicon-content (30 wt%) Si/Gr blends using a decoupled blend cell setup. By analyzing the contributions of individual components, their effective C-rates and charge distribution are assessed throughout the cycling process. The results confirm the nonadditive nature of Si/Gr electrochemistry, demonstrating significant variations in C-rates between silicon and graphite, particularly during delithiation. The study also explores an alternative Si/Gr–Gr decoupled blend setup to better represent lower silicon content electrodes. The findings provide insights into lithium dynamics and the complexities of designing blended electrodes with materials of significantly different specific capacities. This work contributes to the understanding of silicon's role in composite anodes and offers valuable guidelines for designing high-silicon-content electrodes with improved electrochemical performance.

## 1. Introduction

The incremental but steady progress in Li-ion battery performance has broadened its field of application from portable electronics to transportation and beyond. Improving energy density has been a primary research focus, with the use of alloy-based negative electrodes, such as silicon, showing breakthrough prospects thanks to the high achievable capacities. Unfortunately, commercial use remains limited to the addition of a small percentage of silicon to the graphite negative electrode (8%–10% in most cases), as the very high capacity of silicon involves significant volume changes (more than three times) that introduce strains in both the particles and the solid electrolyte interphase (SEI) that cause severe capacity fading.[1–7]

The behavior of graphite and silicon is well known, with each material involving different redox steps associated with the formation of different phases. In graphite, lithium intercalation occurs through a "staging" mechanism, where lithium ions progressively occupy specific interlayers between the carbon layers, allowing for a gradual and controlled increase in lithium concentration during the electrochemical reaction. The stages include Stage IV, (where lithium occupies every fourth interlayer); Stage III, with lithium in every third interlayer; Stage II, (where lithium fills every second interlayer); and finally, Stage I, the fully lithiated phase, in which lithium ions occupy all available interlayer spaces to form $LiC_6$. Stage II corresponds to $Li_{0.5}C_6$, while there are some discrepancies regarding the composition of stages III and IV.[8] In the case of silicon, the mechanism is slightly different depending on whether the starting material is amorphous or crystalline, as crystalline silicon will first transform into an amorphous $Li_xSi$ phase ($0 < \times < 3.75$).[9] Crystalline $Li_{15}Si_4$ will ultimately form at high levels of lithiation (potential below ≈50 mV) in both scenarios. The formation of this phase is typically not fully reversible[10,11] and upon delithiation, the material turns amorphous again.[12] When blending crystalline silicon with graphite, one would expect first lithiation of silicon to produce the amorphous alloy, then lithiation of graphite with formation of stages, and finally formation of $Li_{15}Si_4$ at low potential. Upon oxidation, and due to the lower polarization exhibited by graphite, graphite would delithiate prior to the delithiation of either $Li_{15}Si_4$ or $Li_xSi$.[13]

Despite a large number of papers devoted to the electrochemical characterization of silicon/graphite (from here on denoted Si/Gr) electrodes, prepared by a myriad of techniques and also fabricated using different binders and types of carbon additives, mechanistic studies are more scarce. Meaningful insights were reported by Yao et al.[13] from an operando energy

D. Chatzogiannakis, I. Ghilescu, G. Giannadaki, M. R. Palacin
Institut de Ciència de Materials de Barcelona (ICMAB-CSIC)
Campus UAB, 08193 Bellaterra, Catalonia, Spain
E-mail: rosa.palacin@icmab.es

D. Chatzogiannakis, M. Cabello, M. Casas-Cabanas
Centro de Investigación Cooperativa de Energías Alternativas
(CIC energiGUNE)
Basque Research and Technology Alliance (BRTA)
Alava Technology Park, Albert Einstein 48, 01510 Vitoria-Gasteiz, Spain
E-mail: mcasas@cicenergigune.com

D. Chatzogiannakis
ALISTORE-ERI
CNRS FR
3104 Amiens, France

M. Casas-Cabanas
Ikerbasque - Basque Foundation for Science
Maria Diaz de Haro 3, 48013 Bilbao, Spain

Supporting information for this article is available on the WWW under https://doi.org/10.1002/batt.202500104

Research Article
doi.org/10.1002/batt.202500104
Chemistry Europe
European Chemical Societies Publishing

dispersive X-ray diffraction study in coin cells with electrodes containing 73% of graphite and 15% of Si nanoparticles (wt%) operating at C/30. By quantifying the amount of lithium in the graphite crystalline phases, they were able to confirm the expected mechanism described above, and the differential capacity dQ/dV exhibited the peaks corresponding to both graphite and silicon. Studies devoted to composite electrodes containing Si/Gr blends as active materials have often assumed that the capacities of both materials were simply additive.[14] However, given the distinct redox mechanisms of these materials, this assumption oversimplifies the system. The transfer of lithium between two active materials within the same electrode is well-documented in extensively studied blended positive electrode materials, highlighting the complexity of such interactions.[15–19] Moreover, the possibility of lithium transfer from $LiC_6$ to silicon during relaxation was already discussed by Richter et al. when investigating the aging mechanism and low temperature operation of SiGr electrodes containing 3.5% wt. of micrometric Si[20] and by Berhaut et al.[21] and Frankenstein et al.[22] in electrodes with ≈40% wt. and 80% graphite respectively.

A recent study by Knorr et al. was carried out using two coin cells connected in parallel, each containing a lithium counter electrode, one with $SiO_x$ and the other with graphite as working electrodes, which also enabled the detection lithium transfer during relaxation periods.[23] The redox mechanism of Si/Gr electrodes was investigated by Heubner et al.[24] using the three-electrode experimental setup they developed to study blended positive electrodes.[25] This setup uses a lithium counter electrode and two connected working electrodes, each containing one of the blend components, allowing the measurement of the current flowing between them during cell operation. In that study, a composite electrode containing graphite was used on one side and a sputtered silicon thin film on the other, and the deconvolution of the respective contributions to the capacity confirmed lithium redistribution within the electrode. The results achieved pointed that incorporating silicon to graphite electrodes is beneficial not only in terms of capacity but also in terms of rate capability. Yet, authors called for caution in interpreting the results, as generalization was hampered by the fact that, while a composite electrode similar to those used in real Li-ion cells was used on the graphite side, the behavior of a sputtered thin film may not be fully extrapolatable to silicon containing composite electrodes. Moreover, a comparison with the behavior of composite electrodes containing Si/Gr blends as active material was lacking.

The aim of this work is to build upon the study by Heubner et al.[24] by assessing the representativity of their findings using electrodes that more closely resemble those present in commercial cells. This involves a careful comparison of the trends observed with the three-electrode decoupled blend cell setup with those achieved in conventional coin cells. A previously reported Si/Gr mixture, prepared by a wet ball milling process, along with its individual components, were chosen as references due to the good performance achieved even with high silicon loadings (30% in wt.).[26] Furthermore, owing to the difficulty in preparing composite electrodes with silicon as the only active material, the three-electrode decoupled blend setup was also used with composite electrodes containing a blend active material (Si/Gr) on one working electrode and graphite on the other. The reliability of extrapolating data from this more easily prepared setup to represent that of pure silicon was assessed.

## 2. Results and Discussion

### 2.1. Silicon–Graphite Decoupled Blend

To study the contribution of each blend component as a function of state of charge and compare our findings to those reported by Heubner et al.[24] using a composite electrode, the decoupled blend three-electrode cell was assembled with the two working composite electrodes containing pure silicon and pure graphite as active materials. The active masses of the electrodes used were 4.05 and 1.40 mg for graphite and silicon, respectively, yielding a Si:Gr mass ratio of 26:74, which is very close to that of the reference blended electrode (30:70). The voltage versus capacity profile at C/20 for this decoupled blend setup and the reference coin cell containing the true blended composite electrode as active material are depicted in Figure S7, Supporting Information. Additionally, the corresponding dQ/dV versus voltage plots are also presented. The behaviors are largely similar, the main difference being that the decoupled blend cell setup exhibits higher polarization, as expected. This increased polarization, given that the voltage window remains the same, results in lower capacity. The dQ/dV plots are very similar in both cases and depict the peaks corresponding to the individual blend components (see Figure S7, Supporting Information), thus confirming the representativity of the decoupled blend setup at this rate.

This cell configuration effectively mimics a true blend, allowing for the measurement of the current distribution between each of the two active materials. The voltage of this decoupled blend cell as a function of time is depicted in **Figure 1**. The dark yellow and grey areas represent the amount of charge stored or

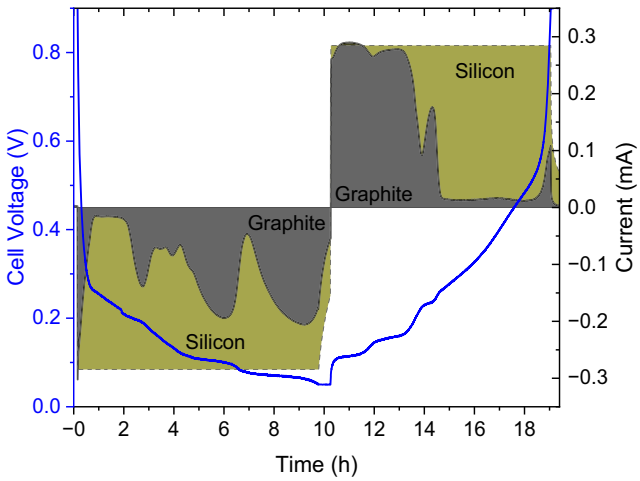


**Figure 1.** Voltage versus time curve of the decoupled blend cell (blue line) and current flowing to/from the graphite electrode (grey line) at C/20. Total cell current is also depicted (thin dashed line). The grey and dark yellow areas indicate the charge distribution between graphite and silicon, respectively. The wt% ratio Gr:Si is 74:26.

Research Article
doi.org/10.1002/batt.202500104
Chemistry Europe
European Chemical Societies Publishing

released by silicon and graphite respectively, and the thin dashed line indicates the total cell current.

The strength of this setup is that it enables to decouple the contribution of each component, as evidenced by the direct observation of their characteristic electrochemical behavior. Notably, the graphite's current fluctuation and peak value differ significantly between the lithiation and the delithiation steps. This is in contrast to the positive electrode blends studied in a previous work[27] and expected from the well-known behavior of silicon and graphite. During lithiation, the activity of graphite exhibits three well-defined peaks that align with the three plateaus that appear on the voltage curve related to stages I, II, and IV. As can be expected, the contribution of graphite increases significantly when the voltage of the cell coincides with the voltage of the plateaus. Two similar current maxima are witnessed at 0.1 and 0.06 V, each corresponding to roughly 70% of the cell's total current. Silicon, in contrast, remains active throughout the whole lithiation process, in agreement with the dQ/dV, exhibiting much broader peaks, and therefore its contribution fluctuates in response to graphite's behavior. This is shown by the fact that silicon's current reaches minima whenever the voltage corresponds to one of the graphite's plateaus. In contrast, during delithiation, the graphite current matches that of the cell until the voltage reaches 0.2 V. This indicates that all lithium extracted from the electrode up to this point originates from graphite, while silicon becomes the dominant active component beyond this voltage. These results are in full agreement with previously reported data on blended silicon graphite electrodes of different formulations derived from operando synchrotron X-ray diffraction (XRD),[13] small and wide-angle X-ray scattering[14] or differential capacity plots.[28] Moreover, this behavior is also similar to the one reported by Heubner et al. for the decoupled blend cell[24] even though the two systems differ significantly. These differences include the type of silicon electrode (thin film vs. composite) and, more importantly, the silicon content (26% vs. 7% Si content). While this is encouraging as it highlights the representativity of the results, it also raises questions about the silicon content effect that may require careful assessment.

Indeed, by measuring the current going to each working electrode and considering the capacity of the respective active materials, the effective C-rate (electrochemical stress) on each component can be calculated at any point of the cycling process. **Figure 2** shows the effective C-rate for both silicon and graphite for the cycle shown in Figure 1. The red dashed line indicates the nominal C-rate, calculated based on the total capacity of the cell. This is determined considering the 1C currents for graphite and silicon as 372 and 4000 mA $g^{-1}$ respectively. As expected, the effective C-rate varies with the state of charge, in agreement with the different dQ/dVs of each component, and also differs between lithiation and delithiation due to the well-known hysteresis of silicon, as mentioned above. From our results it can be observed that graphite exhibits significant deviations from the nominal C-rate. While silicon exhibits an effective rate peak of 0.065 C (C/15) during delithiation, graphite reaches values up to 0.19 C (C/5) which is almost 4 times the cell nominal rate (0.05 C or C/20). The overall fluctuation range on a blend component will not depend on its mass fraction but rather on capacity

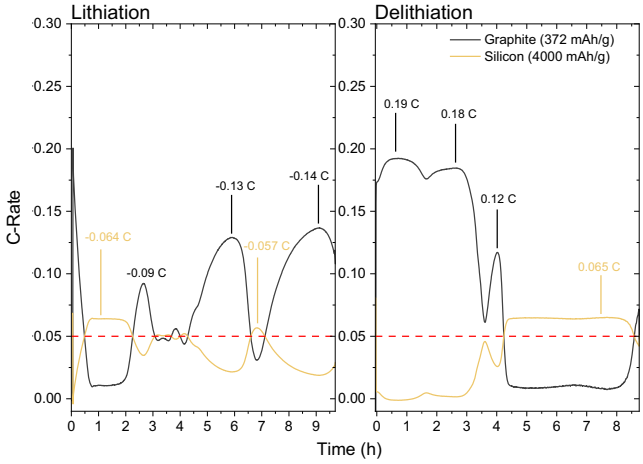


**Figure 2.** Calculated effective C-rate for both graphite (grey lines) and silicon (yellow lines) for the Si-Gr decoupled blend at C/20, with explicit values corresponding to maximum observed C-rates in both lithiation and delithiation. The red dashed line indicates the nominal C-rate of the cell. The wt% ratio of Gr:Si is 74:26.

share. In this case, even though silicon is in significantly lower weight fraction than graphite, its much higher capacity makes it less prone to C-rate fluctuations.

During lithiation, and due to silicon's peaks shifting toward lower potentials, a larger overlap between the two materials´ activities is seen. This overlap allows peak C-rate values to approach the nominal C-rate (although with a larger variation observed for graphite). This indicates that the current is shared between both components, moderating each other's "electrochemical stress". In contrast, during delithiation, the processes of graphite and silicon happen at significantly different potentials, resulting in less overlap. Consequently, graphite handles all of the cell's current at the beginning of the delithiation, which is clearly reflected in the calculated C-rate.

### 2.2. Si/Gr–Gr Decoupled Blend

To understand the effect of blending on the performance of the electrodes, a new setup was assembled, featuring one blended and one unblended working electrode. One was an optimized Si/Gr with 30% silicon content and the other one was a pure graphite electrode. This configuration, referred to as the Si/Gr–Gr cell, was designed to ensure both electrodes had a similar mass loading. Given the significant difference in specific capacities between silicon and graphite, it is not possible to achieve both equal mass loading and capacity simultaneously; therefore this setup prioritizes mass loading consistency.

This approach offers several advantages. First, it avoids the challenges associated with pure silicon electrodes, stemming from its fabrication challenges, which also should result in better performance at elevated rates. Additionally, this setup can simulate a Si/Gr blend of low silicon content without requiring an electrode with extremely low mass loading, which, in the case of silicon is very tricky to make. The resulting silicon content of the system is ≈15 wt%, which also happens to be much closer to the contents used commercially. Details on active material

Research Article
doi.org/10.1002/batt.202500104
Chemistry Europe
European Chemical Societies Publishing

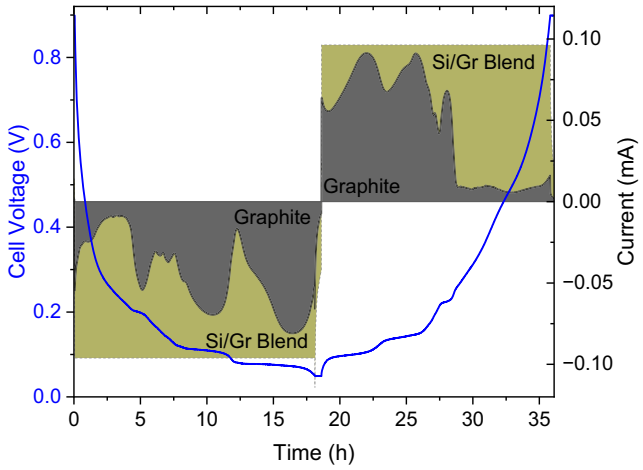


**Figure 3.** Voltage versus time curve of the decoupled blend cell (blue line) and current flowing into graphite (grey line) at C/20 for Si/Gr–Gr cell. Total cell current is also depicted (thin dashed line). The grey and dark yellow areas indicate the charge distribution between graphite and silicon–graphite electrodes, respectively. The wt% ratio Si:Gr is ≈15:85.

quantities and electrode loadings used for this setup and the Si-Gr are included in Table S2, Supporting Information.

**Figure 3** shows the voltage as a function of time for the Si/Gr–Gr cell cycled at C/20. On the same x-axis a thin dashed line indicates the total current delivered to/by the cell. The dark yellow and grey areas represent the amount of charge stored or released by the Si/Gr and Gr electrodes, respectively. Since graphite is present in both electrodes in comparable quantities, its performance and activity during cycling can be directly assessed. Ideally the behavior of silicon could then be inferred by subtracting the graphite contribution, assuming that graphite's response is not significantly altered by the presence of silicon. Thus, comparison with the data depicted in Figure 1 is informative. A very similar behavior during lithiation is observed in both cases, with the current going to the pure graphite electrode bearing the same fluctuations at very similar potentials. In contrast, the behavior is different during the early stages of the delithiation ($V < 0.2$ V). Indeed, a fluctuation of the Gr electrode's current is observed for the Si/Gr–Gr cell, (see Figure S8, Supporting Information). Since it is well known, and observed in Figure 1, that during the early stages of delithiation only graphite is active, the current going to both electrodes should be roughly constant for the Si/Gr–Gr cell. Furthermore, since the amount of graphite is very similar in both pure and blended electrodes 57% and 43%, respectively, a similar current value should be expected for both of them, which is not the case.

In an effort to understand and deconvolute the performance of each material in the cell, further analysis is needed.

Initially, the total current of the cell is the sum of the currents of the two electrodes and as such Equation (1):

$$I_{cell} = I_{Gr}^{pure} + I_{SiGr} \quad (1)$$

and the current of the blended electrode is equal to the sum of the currents of its active components, or Equation (2):

$$I_{cell} = I_{Gr}^{pure} + I_{Gr}^{blended} + I_{Si}^{blended} \quad (2)$$

From this equation, to obtain an analytical result, one has to know the behavior of at least one component of the blended electrode. Since the current distribution of the Si/Gr–Gr decoupled blend cell is overall qualitatively similar to the current measured in the Si-Gr decoupled cell (except for the early stages of delithiation), we hypothesize that graphite in the blended electrode and pure graphite perform equally. In this scenario, the following equation would apply:

$$\frac{I_{Gr}^{pure}}{m_{Gr}^{pure}} = \frac{I_{Gr}^{blended}}{m_{Gr}^{blended}} \quad \text{or} \quad I_{Gr}^{blended} = \frac{m_{Gr}^{blended}}{m_{Gr}^{pure}} I_{Gr}^{pure} \quad (3)$$

Substituting $I_{Gr}^{blended}$ in Equation (2) with its expression from Equation (3) yields:

$$I_{cell} = I_{Gr}^{pure} + \frac{m_{Gr}^{blended}}{m_{Gr}^{pure}} I_{Gr}^{pure} + I_{Si}^{blended} = \left(1 + \frac{m_{Gr}^{blended}}{m_{Gr}^{pure}}\right) I_{Gr}^{pure} + I_{Si}^{blended} \quad (4)$$

$I_{Si}^{blended}$ can be therefore calculated directly from Equation (4) and by applying Equation (2), $I_{Gr}^{blended}$ can be deduced and consequently the total graphite current ($I_{Gr}^{blended} + I_{Gr}^{pure}$). In **Figure 4**, $I_{Gr}$ and $I_{Si}^{blended}$ are depicted alongside with the total cell current ($I_{cell}$) as a function of the voltage.

While the behavior is consistent with expectations based on the study of the Si-Gr blend reported in the previous section, the values of $I_{Gr}$ appear to exceed the total cell current at some points. This is obviously not possible and also results in negative $I_{Si}^{blended}$ calculated values. Thus, the assumption introduced with Equation (3) does not seem to hold, which indicates that the activity of the two types of graphite (blended and nonblended) is different. This is also consistent with the fact that the current on the two electrodes in the region where only graphite is active (delithiation below 0.2 V, see Figure S8, Supporting Information) is

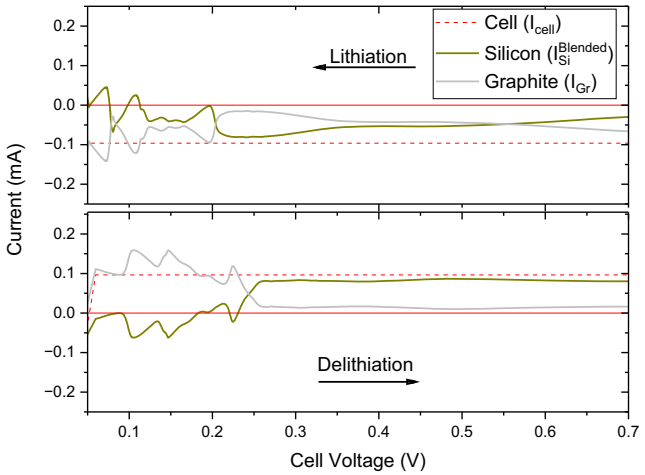


**Figure 4.** Currents calculated using Equations (4) and (2) (see text) for silicon (yellow line) and graphite (grey line) of the Si/Gr–Gr cell at C/20 as a function of cell voltage. Red dashed line represent the total current applied to the cell while the solid red line simply marks zero as a guide to the eye. Same data against time is included as Figure S9, Supporting Information.

Research Article
doi.org/10.1002/batt.202500104
Chemistry Europe
European Chemical Societies Publishing

significantly different despite both electrodes having almost the same graphite content. The phenomenon is especially evident in the first stages of the delithiation, where graphite is subjected to the highest current. The different behavior of graphite when blended might be linked to silicon worsening the electronic/ionic conductivity of the electrode or differences in the SEI formed on Gr and Si/Gr electrodes. Indeed, results derived from studies of nano-Si-filled graphite anode particles point at graphite exhibiting a reduced capacity due to increased polarization derived from the SEI growth on silicon, an effect that will be enhanced at high rates.[28]

### 2.3. Effect of C-Rate and Silicon Content

The experiments depicted above have enabled to assess the effective rate of the blend components during cycling at C/20, which has been proven to significantly fluctuate, peaking at values often many times higher than the nominal one. Given the high hysteresis of silicon, it was deemed useful to assess how these effective rates were modified if the cell nominal rate was increased. In order to assess the representativity of the decoupled blend setup, a set of coin cells, assembled with Si, Gr and Si/Gr, as well as the two decoupled blend cells (Si-Gr and Si/Gr–Gr) were tested at a plethora of rates ranging from C/20–3C. The specific capacities of all the cells during lithiation and delithiation constant current (CC) steps at the different rates are depicted in **Figure 5**.

As expected, the specific capacity decreases with increasing C-rate in all cases, with this decrease being more evident in the lithiation step. Interestingly, and probably due to partial particle disconnection, the pure silicon electrode´s capacity decays very quickly and, for the lithiation, reaches zero for rates higher than 1C. Both the Si/Gr blend as well as the graphite coin cells still deliver satisfactory capacity values up to 3C, with graphite appearing the most unaffected. Yet, and given the higher polarization derived from the decoupled blend cell, it comes as no surprise that the Si-Gr decoupled blend cell capacity does also reach zero at 1C during lithiation. In contrast, the Si/Gr–Gr cell is able to provide some capacity up to 3C. The 1C cycle was deemed the most relevant to analyze, and the amount of charge stored or released by the Si/Gr and graphite electrodes, respectively at this rate is shown in **Figure 6**.

Compared to Figure 3, corresponding to the same system at C/20, it is interesting to note that at 1C the characteristic peaks related to the staging of graphite can still be inferred, despite being less well defined. The lowest voltage peak of graphite during lithiation is not clearly observed, as the cutoff potential is reached before due to larger cell polarization. Yet, and due to the existence of the constant voltage step ($0.55\ h < t < 1.05\ h$), lithiation continues, and as such the peak is observed during delithiation. The specific currents, $I_{Si}^{blended}$ and $I_{Gr}$ are depicted in **Figure 7**, again under the assumption of Equation (3). Despite the current of graphite ($I_{Gr}$) exceeding its allowed limits, as observed at C/20 (Figure 4), it is interesting to note that at this

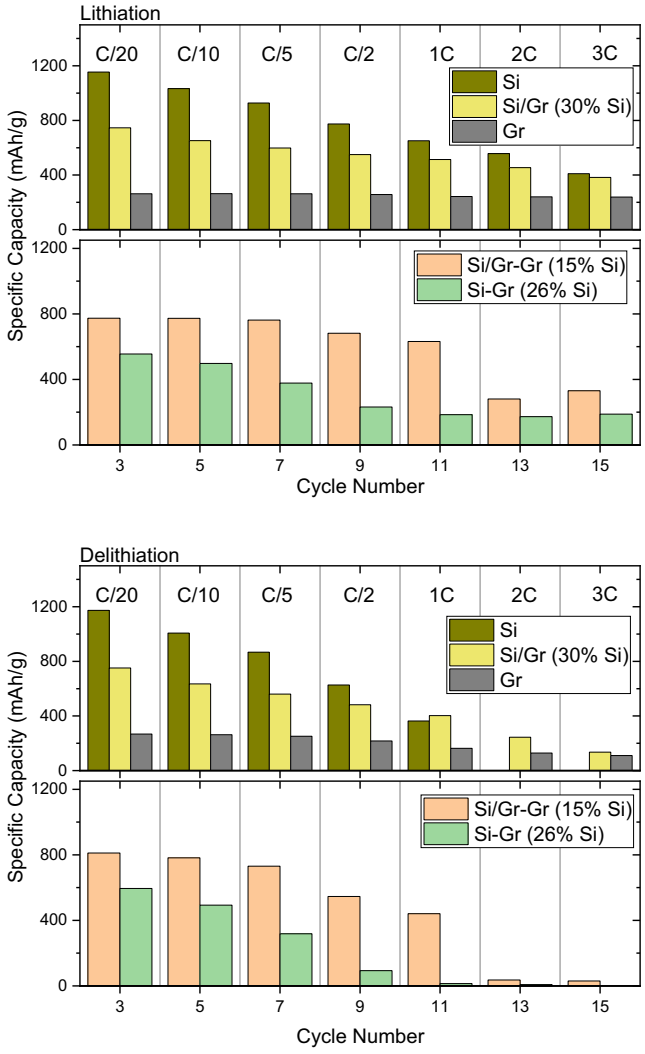


**Figure 5.** Specific capacities for lithiation (top) and delithiation (bottom) at rates from C/20 up to 1C. Values are calculated taking into account only the CC part. The second cycle from each sequence is depicted.

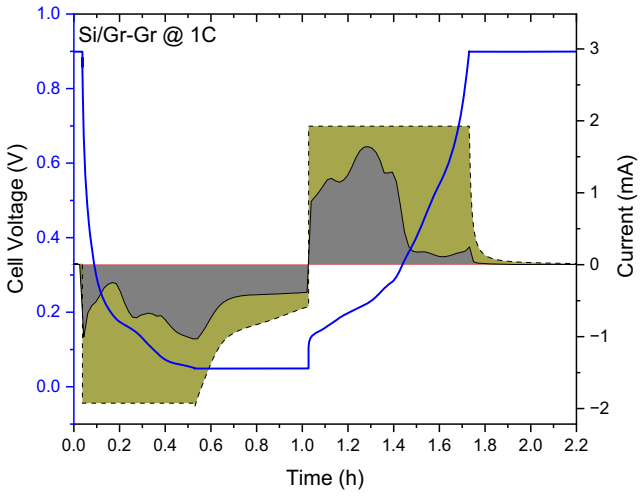


**Figure 6.** Voltage versus time curve of the decoupled blend cell (blue line) and current flowing into the Gr electrode (grey line) at 1C for the Si/Gr–Gr cell (cycle 11 from Figure 5). Total cell current is also depicted (thin dashed line). The grey and dark yellow areas indicate the charge distribution between Gr and Si-Gr electrodes respectively.

Research Article
doi.org/10.1002/batt.202500104
Chemistry Europe
European Chemical Societies Publishing

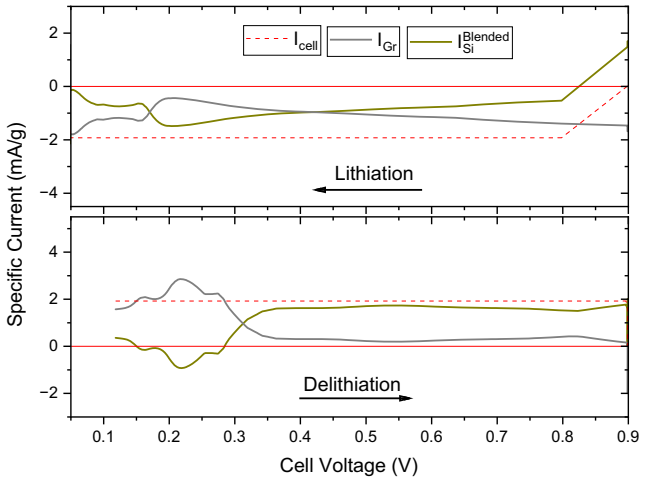


**Figure 7.** Currents calculated using Equation (4) and (2) (see text) for silicon (yellow line) and graphite (grey line) of the Si/Gr–Gr cell at 1C as a function of cell voltage. Red dashed line represent the total current applied to the cell while the solid red line simply marks zero as a guide to the eye.

rate, this is only visible during the delithiation process, and again, in the areas where graphite is most active. Since graphite does exhibit faster kinetics, it will always be active in the beginning of the delithiation and hence the anomaly is seen at both rates. On the contrary, during lithiation, silicon and graphite are active at the same time and the effect is not seen at faster rates, implying that rate seems to reduce the error imposed by Equation (2). Yet, the results of both experiments point at the behavior of graphite being different in pure and in blended electrodes.

## 3. Conclusion

This study investigates the behavior of Si/Gr blended composite electrodes, commonly used as negative electrodes in commercial Li-ion batteries, using a decoupled blend setup, to explore the electrochemical interactions between silicon and graphite. High silicon content blends (26% of the total active material mass) were studied, together with electrodes containing only the individual components. Coin cell experiments with both blended and pure electrodes provided reference data, revealing consistent results. The blended electrode exhibited the characteristic features of both constituents, with notable differences observed between lithiation and delithiation steps. The decoupled approach enables the separation of individual component contributions, revealing significant fluctuations in effective C-rates, particularly for graphite during delithiation. A significant discrepancy in effective C-rates between silicon and graphite, which varies with the state of charge, was identified. Despite being the majority component, graphite experiences a notably higher rate than the nominal value due to the substantial difference in specific capacity between the two materials. This contrasts with the situation in blended positive electrodes, where the components have much more similar capacity values. Overall, increasing the silicon fraction intensifies the stress on graphite, which could result in accelerated graphite degradation and/or worse performance and must be taken into consideration if high silicon content Si/Gr blends are to be commercially implemented. This significant difference in capacities for both blend components would also preclude the study of low silicon content Si/Gr blends using the decoupled blend cell. Yet, an effort was made through the use of Si/Gr electrodes in the setup. The Si/Gr–Gr configuration at C/20 offers the most accurate representation of real blend behavior and remains largely valid at 1C, confirming its relevance for practical applications. It was found that the deconvolution of the component currents is not trivial, most likely due to the difference in the activity of graphite when blended or when alone. This anomaly was always observed in the delithiation step, yet only in the slow lithiation. In summary, these findings emphasize the complexity of lithium distribution in blended electrodes and its dependence on rate and blending ratio and underscore the need for precise component balancing in silicon–graphite anodes for next-generation Li-ion batteries. This is particularly crucial when incorporating higher fractions of silicon to meet increasing energy density demands.

## 4. Experimental Section

### Electrode Fabrication

The graphite electrode was cast using a protocol adapted from one used for positive electrodes using N-Methyl-2-pyrrolidone (NMP, Sigma-Aldrich) as a solvent, polyvinylidene fluoride, PVDF (Solvay) binder and C65 carbon additive (Imerys). Initially, a 5%wt. solution of the binder was made using magnetic stirring. The graphite powder used was also purchased from Imerys ($D50 = 12–13\ \mu m$). The graphite and C65 powders were premixed and then added to a previously weighted amount of the binder solution while vigorously stirring using a high shear mixer (T 25 digital ULTRA-TURRAX, IKA) until a homogeneous slurry was obtained. A small amount of pure NMP was added during this process to adjust the viscosity. Amorphous silicon nanoparticles (Alfa-Aesar) with diameters of less than 50 nm were used for the silicon composite electrodes. In this case, electrodes were cast from a water-based slurry using lithium polyacrylic acid (Li-PAA).[29] In order to prepare the slurry, the carbon additive and silicon nanoparticles were initially ball-milled for 20 min prior to their use. After that, the process followed was identical to the one described above for graphite using water instead of NMP. Most electrodes fabricated with pure silicon faced issues such as partial dewetting after casting or delamination and cracking of the film from the copper substrate after drying. To address these issues, adjustments were made to the slurry viscosity and tape casting, namely quantity of solvent and coating speed, which enabled some improvement. The best electrodes had enough adhesion to be assembled and tested, delivering satisfactory electrochemical performance despite still exhibiting some surface cracking. The silicon–graphite (Si/Gr) composite electrode is described in reference,[26] with few layer graphene being used as conducting additive. All the electrodes prepared contained 80% wt. active material 10% wt. binder and 10% wt. carbon additive. Its active mass was comprised of 30% wt. silicon and 70%wt. graphite. Scanning Electron Microscopy images and XRD patterns of the electrodes and the active materials are included in the supporting information (Figure S1–5, Supporting Information) and were taken with a FEI Quanta 200 ESEM FEG microscope and a Bruker D8 Advance A25 X-ray diffractometer ($\lambda = 0.7093$ Å) respectively.

### Electrochemical Testing

To prepare CR2032 coin cells, all components were first dried at 70 °C to remove any moisture. Electrodes with a diameter of 14 mm were punched from the prepared laminates, and their mass was reported in Table S1, Supporting Information. The punched electrodes were then dried in a vacuum oven at 120 °C for at least 1 h. After drying, both the coin cell parts and electrodes were transferred to an argon filled glove box where the cell assembly took place. Lithium metal was used as a counter electrode and Whatman borosilicate glass fiber filter, soaked with electrolyte (1 M $LiPF_6$ in EC:DMC) as separator.

The three electrode "decoupled blend" cell setup assembly and electrical connection were described in detail in[19] and was based on the method developed by Heubner et al.[25] bearing a lithium metal counter electrode between two working electrodes, that were maintained at the same potential using a potentiostat channel ($\Delta V = 0$ V). During testing, the current flowing to/from each working electrode was recorded.

All the electrochemical tests were conducted using a VMP3 (Biologic, France). Cells underwent an initial formation cycle down to 0.005 V versus $Li/Li^+$ and were subsequently cycled between 0.05 and 0.9 V at room temperature (≈25 °C). The protocol was derived from previous studies,[26] with the first cycle involving a shallow reduction to promote the formation of the SEI, but further keeping the potential above 50 mV, to avoid the formation $Li_{15}Si_4$ which could be detrimental for cycling.[9] Analysis of the dQ/dV plots for the first formation cycle indicates that a small amount of $Li_{15}Si_4$ might form in the electrodes on the first shallow reduction, that reacts upon further oxidation (Figure S6, Supporting Information) and therefore should not overall impact the assessment of the effective rates and lithium dynamics presented herein. Initial coulombic efficiency for the first cycle ranged from 66% for the pure silicon electrode to 75% for the pure graphite electrode. The data reported for the decoupled blend cell correspond to cycle number 2 or 3 at C/20 and cycle 11 at 1C rate. Cells were tested in a CC-CV mode, with a 1 h constant voltage step at the end of lithiation/delitiation at the corresponding cutoff voltage.

## Acknowledgements

This work has been done in the framework of the doctorate in Materials Science of the Universitat Autònoma de Barcelona. D.C. wants to acknowledge DESTINY MSCA PhD Programme, which has received funding from the European Union's Horizon 2020 research and innovation programme under grant agreement no 945357. ICMAB-CSIC members thank the Spanish Agencia Estatal de Investigación Severo Ochoa Programme for Centres of Excellence in R&D (CEX2023-001263-S) and funding through grant PID2023-146263NB-I00. MCC thanks grant PID2022-137626OB-C33 funded by MICIU/AEI/10.13039/501100011033 and by "ERDF A way of making Europe". Authors acknowledge the use of an image from Flaticon.com (gas pedal) for the ToC image.

## Conflict of Interest

The authors declare no conflict of interest.

## Data Availability Statement

The data that support the findings of this study are available from the corresponding author upon reasonable request.

**Keywords:** blend electrodes · electrochemistry · Li-ion batteries · redox chemistry · silicon/graphite electrodes

[1] K. Feng, M. Li, W. Liu, A. G. Kashkooli, X. Xiao, M. Cai, Z. Chen, *Small* **2018**, *14*, 1702737.
[2] Y. Jin, B. Zhu, Z. Lu, N. Liu, J. Zhu, *Adv. Energy Mater.* **2017**, *7*, 1700715.
[3] S. Chae, S. H. Choi, N. Kim, J. Sung, J. Cho, *Angew. Chem., Int. Ed.* **2020**, *59*, 110.
[4] U. Kasavajjula, C. Wang, A. J. Appleby, *J. Power Sources* **2007**, *163*, 1003.
[5] H. Takezawa, S. Ito, H. Yoshizawa, T. Abe, *J. Power Sources* **2016**, *324*, 45.
[6] H. Wu, Y. Cui, *Nano Today* **2012**, *7*, 414.
[7] L. Martin, H. Martinez, M. Ulldemolins, B. Pecquenard, F. Le Cras, *Solid State Ion* **2012**, *215*, 36.
[8] M. Winter, J. O. Besenhard, *Handbook of Battery Materials*, Vol.*1*, 2nd ed., Wiley-VCH, Weinheim, Germany, **2011**.
[9] M. N. Obrovac, V. L. Chevrier, *Chem. Rev.* **2014**, *114*, 11444.
[10] M. N. Obrovac, L. J. Krause, *J. Electrochem. Soc.* **2007**, *154*, A103.
[11] J. Li, J. R. Dahn, *J. Electrochem. Soc.* **2007**, *154*, A156.
[12] S. Srivastava, J. L. Schaefer, Z. Yang, Z. Tu, L. A. Archer, *Adv. Mater.* **2014**, *26*, 201.
[13] K. P. C. Yao, J. S. Okasinski, K. Kalaga, J. D. Almer, D. P. Abraham, *Adv. Energy Mater.* **2019**, *9*, 1803380.
[14] C. L. Berhaut, D. Z. Dominguez, P. Kumar, P. H. Jouneau, W. Porcher, D. Aradilla, S. Tardif, S. Pouget, S. Lyonnard, *ACS Nano* **2019**, *13*, 11538.
[15] A. J. Smith, S. R. Smith, T. Byrne, J. C. Burns, J. R. Dahn, *J. Electrochem. Soc.* **2012**, *159*, A1696.
[16] H. Y. Tran, C. Täubert, M. Wohlfahrt-Mehrens, *Prog. Solid State Chem.* **2014**, *42*, 118.
[17] C. Heubner, U. Langklotz, A. Michaelis, *J. Energy Storage* **2018**, *15*, 181.
[18] M. Casas-Cabanas, A. Ponrouch, M. R. Palacín, *Isr. J. Chem.* **2021**, *61*, 26.
[19] D. Chatzogiannakis, M. Fehse, M. A. Cabañero, N. Romano, A. Black, D. Saurel, M. R. Palacin, M. Casas-Cabanas, *J. Power Sources* **2024**, *591*, 233804.
[20] K. Richter, T. Waldmann, N. Paul, N. Jobst, R. G. Scurtu, M. Hofmann, R. Gilles, M. Wohlfahrt-Mehrens, *ChemSusChem* **2020**, *13*, 529.
[21] C. L. Berhaut, M. Mirolo, D. Z. Dominguez, I. Martens, S. Pouget, N. Herlin-Boime, M. Chandesris, S. Tardif, J. Drnec, S. Lyonnard, *Adv. Energy Mater.* **2023**, *13*, 2301874.
[22] L. Frankenstein, P. Jan Glomb, M. Mohrhardt, S. Böckmann, L. Focks, A. Gomez-Martin, T. Placke, M. Ryan Hansen, M. Winter, J. Kasnatscheew, *ChemSusChem* **2024**, e202401290.
[23] J. Knorr, J. Li, M. Schamel, T. Kufner, A. Adam, M. A. Danzer, *J. Electrochem. Soc.* **2024**, *171*, 080512.
[24] C. Heubner, T. Liebmann, O. Lohrberg, S. Cangaz, S. Maletti, A. Michaelis, *Batter. Supercaps* **2022**, *5*, e202100182.
[25] C. Heubner, T. Liebmann, C. Lämmel, M. Schneider, A. Michaelis, *J. Energy Storage* **2018**, *20*, 101.
[26] M. Cabello, E. Gucciardi, A. Herrán, D. Carriazo, A. Villaverde, T. Rojo, *Molecules* **2020**, *25*, 2494.
[27] D. Chatzogiannakis, V. Arszelewska, P. E. Cabelguen, F. Fauth, M. Casas-Cabanas, M. R. Palacin, *Energy Storage Mater.* **2024**, *69*, 103414.
[28] H. Jiang, M. Salehabadi, S. Yasmin, J. Wang, M. N. Obrovac, *J. Electrochem. Soc.* **2023**, *170*, 120511.
[29] N. P. W. Pieczonka, V. Borgel, B. Ziv, N. Leifer, V. Dargel, D. Aurbach, J. H. Kim, Z. Liu, X. Huang, S. A. Krachkovskiy, G. R. Goward, I. Halalay, B. R. Powell, A. Manthiram, *Adv. Energy Mater.* **2015**, *5*, 1501008.

Manuscript received: February 13, 2025
Revised manuscript received: April 2, 2025
Version of record online: April 25, 2025